Water-Soluble Lacunary Polyoxometalates with Excellent Electron Mobilities and Hole Blocking Capabilities for High Efficiency Fluorescent and Phosphorescent Organic Light Emitting Diodes

*Marinos Tountas, Yasemin Topal, Mahmut Kus, Mustafa Ersöz, Mihalis Fakis, Panagiotis Argitis, and Maria Vasilopoulou**

High performance solution-processed fluorescent and phosphorescent organic light emitting diodes (OLEDs) are achieved by water solution processing of lacunary polyoxometalates used as novel electron injection/transport materials with excellent electron mobilities and hole blocking capabilities. Green fluorescent OLEDs using poly[(9,9-dioctylfluorenyl-2,7-diyl)-co-(1,4-benzo-{2,1′,3}-thiadiazole)] (F8BT) as the emissive layer and our polyoxometalates as electron transport/hole blocking layers give a luminous efficiency up to 6.7 lm W^{-1} and a current efficiency up to 14.0 cd A^{-1} which remained nearly stable for about 500 h of operation. In addition, blue phosphorescent OLEDs (PHOLEDs) using poly(9-vinylcarbazole) (PVK):1,3-bis[2-(4-tert-butylphenyl)-1,3,4-oxadiazo-5-yl]benzene (OXD-7) as a host and 10.0 wt% FIrpic as the blue dopant in the emissive layer and a polyoxometalate as electron transport material give 12.5 lm W^{-1} and 30.0 cd A^{-1} power and luminous efficiency, respectively, which are among the best performance values observed to date for all-solution processed blue PHOLEDs. The lacunary polyoxometalates exhibit unique properties such as low electron affinity and high ionization energy (of about 3.0 and 7.5 eV, respectively) which render them as efficient electron injection/hole blocking layers and, most importantly, exceptionally high electron mobility of up to 10^{-2} cm^2 V^{-1} s^{-1}.

1. Introduction

Organic light-emitting diodes (OLEDs) have been extensively investigated over the past decades as a promising technology for flat-panel displays and solid-state lighting because of their low cost, light weight, large viewing angle, and mechanical flexibility.[1–5] To date, highly efficient OLEDs are mainly based on phosphorescent emitters which can convert both singlet and triplet excitons into photons and have resulted in 100% internal quantum efficiency.[6–12] Nevertheless, despite the large efficiency enhancement in current state-of-the-art devices, both fluorescent and phosphorescent OLEDs still have considerable room for improvement in the device efficiency and stability needed for commercial applications. In addition, OLEDs have encountered enormous difficulties in meeting the low-cost, high-resolution requirements for large-sized devices due to a limitation in vacuum thermal evaporation technology. Therefore solution processes have drawn a considerable amount of attention as an alternative for production because they allow low-cost, large-area manufacturing. Regarding the performance enhancement, one of the parameters required to achieve high electroluminescence efficiency in OLEDs is to have a balanced charge injection and transport throughout the emissive layer, which increases the probability of two charges of opposite sign recombining far from the electrodes and avoids quenching of radiative charge recombination by the electrodes.[13] The most important way to obtain a good charge balance and improve performance, including also the long-term stability of OLED devices, is by using various types of layers, such as hole injection layers (HILs), hole transport layers (HTLs), electron blocking layers (EBLs), hole blocking layers (HBLs), electron transport layers (ETLs) and electron injection layers (EILs).[14–17] In typical heterojunction OLEDs, however, the mobility of holes is larger than that of electrons and hole injection barrier is lower than electron injection barrier. Such devices have extra holes in the emission region and electrons are more or less consumed before reaching the emissive layer, which decreases the device efficiency. An effective approach is thus the simultaneous

M. Tountas, Dr. P. Argitis, Dr. M. Vasilopoulou
Institute of Nanoscience and Nanotechnology (INN)
National Center for Scientific Research "Demokritos"
Athens, Greece
E-mail: m.vasilopoulou@inn.demokritos.gr
Y. Topal, Prof. M. Kus, Prof. M. Ersöz
Advanced Technology Research & Application Center
Selcuk University
Konya, Turkey
Prof. M. Fakis
Department of Physics
University of Patras
Rio, Patra, Greece

DOI: 10.1002/adfm.201504832

incorporation of an ETL, a HBL, and an EIL between the emissive layer (EML) and metal cathode which, however, increases the device complexity. In this aspect, it is difficult to obtain all solution-processed highly efficient and stable devices with a perfect charge balance because the multilayer stacking of the functional materials by a solution process is almost impossible due to interfacial mixing between organic layers.[18,19] The main reason for such difficulty is the lack of materials with perfect orthogonality in solubility, which typically causes a mixing of the polymeric or small molecular species at the interface of the functional layers during the successive solution processes. It is therefore highly desirable to use electron transport materials (ETMs) which ideally combine a low electron affinity to enable efficient electron injection, a high electron mobility to enhance electron flux, a high ionization energy to act as effective hole blocking layers, the ability to confine excitons within the emissive layer and orthogonal sequential solution processability on multilayered structures.[20–23] Nowadays, to improve electron injection/transport, vacuum-deposited low work function metals, e.g., Li, Mg, and Ca or thin halide layers, e.g., LiF and CsF, are inserted between the EML and cathode metals such as Al or Ag.[24–27] However, subsequent deposition of cathode material, e.g., Al, is accompanied by an uncharacterized reaction with LiF and CsF, Li, Mg, and Ca which react with and diffuse into the polymer and, in addition, are sensitive to ambient water and oxygen. It is also reported that the electron injection can be improved by inserting cesium compounds (e.g. cesium carbonate, Cs_2CO_3) between organic material and Al.[28,29] Also, various n-type metal oxide films such as ZnO, TiO_2, and ZrO_2 have been employed as ETMs in fluorescent OLEDs with an inverted structure,[30–33] whereas various other strategies have been also applied to promote electron injection and transport between the metal cathode and the EML by using an interlayer, such as conjugated polyelectrolytes,[34–37] self-assembled dipole monolayer,[38,39] porphyrin,[40] or phthalocyanine compounds.[41] In addition, imine-nitrogen rich heterocyclic molecules capable of high electron mobility are of increasing interest in developing efficient ETMs for phosphorescent OLEDs,[42,43] whereas pyridine-containing benzene derivatives, which possess both high electron mobility and low electron affinity, have also been reported.[44] However, most of these materials do not meet all the criteria required for an ideal ETM—for instance, organic materials which exhibit orthogonal solution processability show usually poor charge transport properties and may also affect adversely the device lifetime—and therefore the development of new ETMs with optimum properties for next generation OLEDs, is deemed necessary.

On the other hand, polyoxometalates (POMs) are fully inorganic, discrete anionic metal oxygen clusters which can be regarded as soluble oxide fragments.[45–49] They exhibit a great diversity of sizes, nuclearities, and shapes. While these species have been known for almost two centuries, they still attract much interest partly based on their diverse domains of applications.[50–54] Recently, our group proposed the use of solution-processable POMs exhibiting either the Keggin or the Dawson structure as novel electron injection layers with an appropriately located band between the polymer lowest unoccupied molecular orbital (LUMO) and the Fermi level of Al, which was formed via the solid state reduction of POMs by an Al cathode in order to enhance electron injection.[55,56] The high degree of these POMs reduction by Al was found to be of vital importance in obtaining effective electron transport through the cathode interface. However, their low lying conduction band edge limits their use in OLEDs using a diverse range of emissive layers.

In this paper, two different types of water-soluble POMs exhibiting the lacunary Keggin structure, in particular the potassium sodium 11-tungstendiphosphate (α-$K_{7-x}Na_xPW_{11}O_{39}\cdot 14H_2O$) termed hereafter as B1-W and the potassium sodium 11-molybdodiphosphate (α-$K_{7-x}Na_xPMo_{11}O_{39}\cdot 14H_2O$) termed hereafter as B1-Mo, are proposed as highly effective ETMs in all solution-processed fluorescent and phosphorescent OLEDs exhibiting high efficiencies and stabilities. In particular, green fluorescent OLEDs using poly[(9,9-dioctylfluorenyl-2,7-diyl)-co-(1,4-benzo-{2,1′,3}-thiadiazole)] (F8BT) as the emissive layer and B1-Mo as the ETM gave a luminous efficiency up to 6.7 lm W^{-1} and a current efficiency up to 14.0 cd A^{-1} which remained nearly stable for more than 500 h of operation. These values are significantly higher (40%) than those for the corresponding reference device incorporating a Cs_2CO_3-doped ZnO electron injection layer. In addition, blue PHOLEDs using poly(9-vinylcarbazole) (PVK):1,3-bis[2-(4-tert-butylphenyl)-1,3,4-oxadiazo-5-yl]benzene (OXD-7) (PVK:OXD-7 = 60:40, wt/wt) as a host and 10.0 wt% FIrpic as the blue dopant in the emissive layer and B1-Mo as the ETM gave 12.5 lm W^{-1} and 30.0 cd A^{-1} , power and luminous efficiency, respectively. All the above values are among the highest efficiencies reported for a thin F8BT film based OLED and an PVK:OXD-7:FIrpic based PHOLED, respectively, indicating the effectiveness of our lacunary POMs as ETMs. This is mainly a result of their excellent electron mobility, which in the case of B1-Mo was found up to 10^{-2} cm^2 V^{-1} s^{-1} , representing one of the highest mobilities ever reported for a solution processed EMT used in OLED devices, and the low electron affinity and high ionization energy values (about 3.0 and 7.5 eV, respectively), which successfully promoted their electron-injection and hole-blocking behavior.

2. Results and Discussion

Figure 1a provides illustration of the OLED devices structure, including the transport layer used to enhance hole transport, the emissive (EML) and the ETL layer, respectively. The fluorescent OLEDs were fabricated on indium tin oxide (ITO) substrates via the sequential deposition of the solution processed MoO_x, F8BT, and POM layers, which served as the HTL, the EML, and the ETL, respectively. The preparation of s-MoO_x was previously reported,[57] whereas B1-W and B1-Mo were prepared as described in the literature and their purity was checked by ^{31}P nuclear magnetic resonance (NMR) and infrared (IR) spectroscopy (Figures S1 and S2, Supporting Information).[58] In addition, reference devices using 10-nm thick film consisting of Cs_2CO_3-doped ZnO nanoparticles (termed hereafter as ZnO:Cs_2CO_3), which served as the EIL/ETL on the device configuration to improve the electron injection from the Al cathode to the LUMO of F8BT, were fabricated according to the literature procedure.[59,60] The PHOLEDs were fabricated via the sequential deposition of s-MoO_x (HTL), PVK:OXD-7:FIrpic (EML) and the POM film which served as

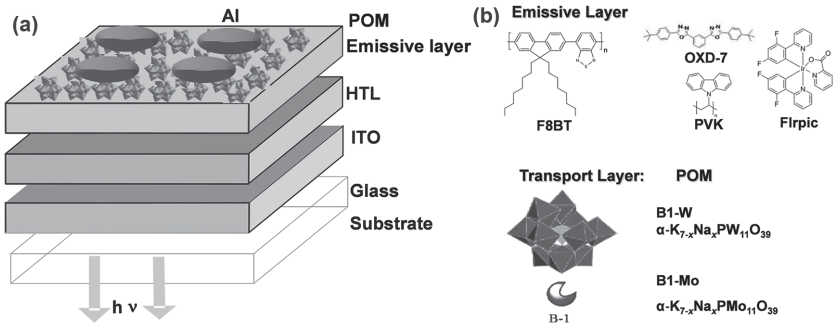

Figure 1. a) Schematic illustration of the OLED devices. b) The chemical structures of the materials used in the emissive layers and of the lacunary POMs used.

the electron injection/transport layer. The reference devices employed a 20-nm thick ETL based on 1,3,5-tris(m-pyrid-3-yl-phenyl)benzene (TmPyPB) doped with Cs_2CO_3 (termed hereafter as TmPyPB:Cs_2CO_3).[20] The concentration of the dopant in the ETL was 7.5 wt% Cs_2CO_3. Additional information on the devices fabrication is included in the Experimental Section. Note that the selection of ZnO:Cs_2CO_3 and TmPyPB:Cs_2CO_3 for use as EILs/ETLs in the reference devices was due to their well-established electron injection capabilities which previously permitted the fabrication of high performing F8BT-based fluorescent OLEDs and PVK:OXD-7:FIrpic-based PHOLEDs, respectively.[20,59]

Figure 1b illustrates the chemical structures of F8BT, PVK, OXD-7, and FIrpic compounds, used in the emissive layers of OLEDs. The chemical structures of B1-W and BI-Mo polyoxometalates are also presented. These are the so-called "lacunary" or "defect" derivatives of the α-Keggin structures that are obtained by removal of one MO_6 (M = W, Mo) octahedron. Since oxygen atoms are shared between polyhedra, removal of a MO_6 octahedron results in stoichiometric loss of an MO^{4+} group from the complete anion. In addition, these POMs are expected to exhibit significant local surface charge density due to their distorted structure which results in asymmetrical distribution of positive and negative charges. The above may have significant impact on their electronic properties and, consequently, on the device operational characteristics, as discussed below.

The results from the characterization of the fluorescent devices with different ETLs (B1-W, B1-Mo, and ZnO:Cs_2CO_3) are presented in **Figure 2** and **Table 1**. (Note that an initial study to determine the suitable thickness of POM films in order to achieve optimum device performance was carried out.

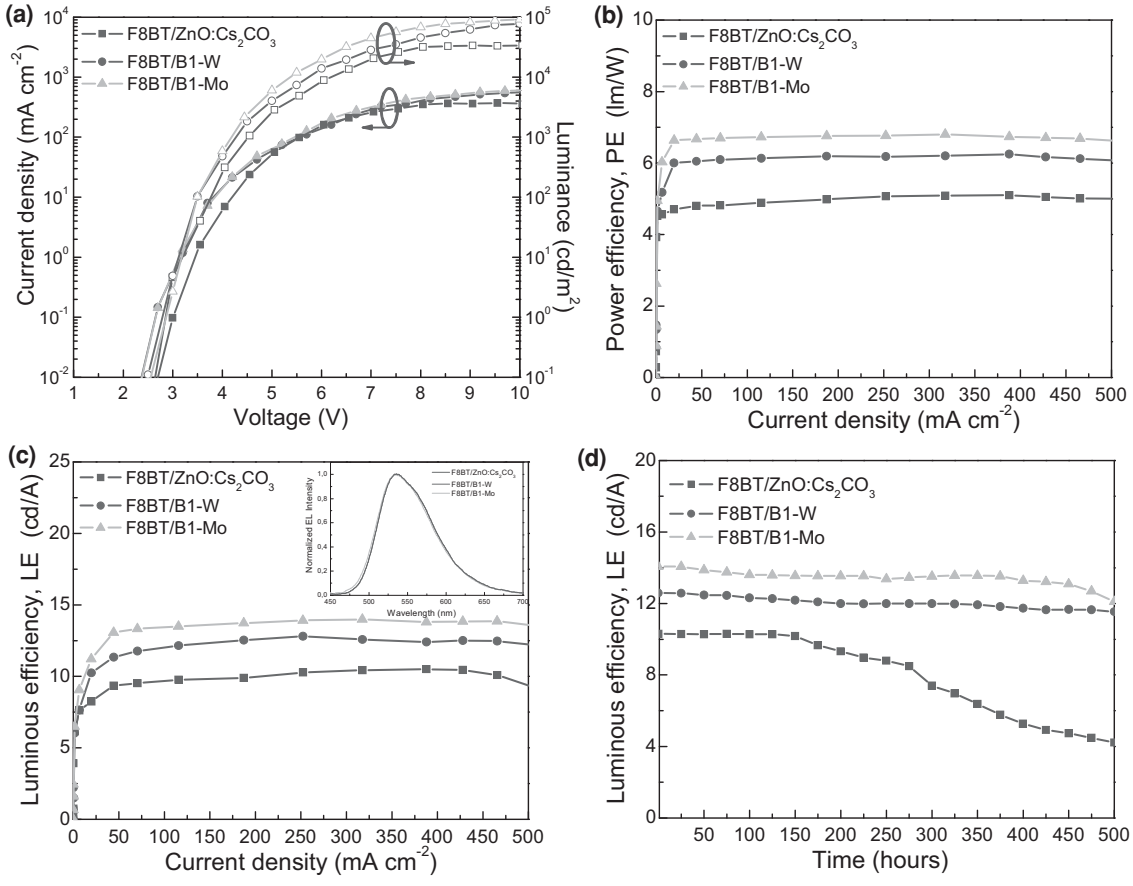

Figure 2. a) Current density and luminance versus voltage (*J*–*V*–*L*) characteristics, b) power efficiency, and c) luminous efficiency versus current density of the F8BT based OLEDs. The EL spectra are shown as inset. d) Stability study: luminous efficiency versus time of the same devices.

Table 1. Device characteristics of fluorescent OLEDs having the structure ITO/MoO_x/F8BT/POM or ZnO:Cs_2CO_3/Al.

ETM	$V_{turn\text{-}on}$ [V] [at 1 cd m^{-2}]	J_{max} [mA cm^{-2}]	L_{max} [cd m^{-2}]	LE_{max} [cd A^{-1}]	PE_{max} [lm W^{-1}]	EQE_{max} [%]
ZnO:Cs_2CO_3	3.2	550	55 000	10.0	4.8	3.4
B1-W	2.8	670	85 000	12.7	6.1	4.3
B1-Mo	2.6	700	98 000	14.0	6.7	4.8

J–V–L measurements taken in OLED devices and presented in Figure S3 (Supporting Information) revealed that by using a solution with a concentration of 20 mg mL^{-1}, which gave a film with a thickness of 20 nm, we obtained the best performance of our devices. In addition, the solution with the concentration of 20 mg mL^{-1} gave better coverage of the F8BT film with a POM film consisting of dense nanostructures, as shown in Figure S4 (Supporting Information)). The presented data in Figure 2 include current density and luminance versus voltage (*J–V–L*) characteristics (Figure 2a), power efficiency versus applied voltage (*PE–V*, Figure 2b), luminous efficiency versus applied voltage (*LE–V*, Figure 2c), and *LE* versus time (stability study, Figure 2d). The efficiencies of the OLEDs for the three different ETLs include PEs 6.1 lm W^{-1} (B1-W), 6.7 lm W^{-1} (B1-Mo), and 4.8 lm W^{-1} (ZnO:Cs_2CO_3), LEs 12.7 cd A^{-1}, 14.0 cd A^{-1}, and 10.0 cd A^{-1}, and external quantum efficiencies (EQEs) 4.3%, 4.8%, and 3.4%, respectively. The PEs of the devices with the B1-W and B1-Mo are 27% and 40%, respectively, higher than those of the reference one although the reference device is already well-performing.

Such efficiency enhancement can be attributed to a significant enhancement of electron injection/transport rates,[61,62] as was supported by measurements in electron only F8BT devices with the structure Al/F8BT/POM or ZnO:Cs_2CO_3/Al (Figure S5, Supporting Information). The current densities of all electron only devices are high but those with POMs are higher than that of the reference device with ZnO:Cs_2CO_3 (especially at low voltages). This result clearly demonstrates that the electron injection and transport in POM bearing devices are enhanced which could be a result of high electron mobilities and favorable energy levels, as will be discussed in detail below. The normalized electroluminescence (EL) spectra of our devices are presented as inset in Figure 2c. Interestingly, all emission patterns of the F8BT based OLEDs with the different ETMs are similar to the photoluminescence and electroluminescence spectra of pristine F8BT (Figure S6, Supporting Information).

Note that stability studies were also performed highlighting also the ability of POMs to act as protecting layers. The above OLEDs were stored in a N_2-filled glovebox without encapsulation, and their performance was measured after certain time intervals (24 h) at ambient conditions. The LE values of the three devices are plotted as a function of the store time in Figure 2d. The devices with the POM materials retained nearly the same luminous efficiency even after 500 h of operation whereas the reference one exhibited nearly 50% of its initial efficiency when operated under the same conditions and for the same time period as the POM bearing devices, which was already significantly improved in comparison with the device with an unmodified cathode which lost 100% of its efficiency in only few days of operation (results not shown). These results demonstrate the ability of POM to also act as buffer layers offering high resistance against the several degradation mechanisms of the OLED devices.

Next, in order to probe possible changes in exciton lifetimes when using different ETMs, photoluminescence spectroscopy was used. The steady state photoluminescence (PL) spectra of F8BT deposited on the three different substrates, in particular ZnO:Cs_2CO_3, B1-W, and B1-Mo, are presented in **Figure 3**a. As in the case of the electroluminescence spectra, again all PL emission features of the F8BT layer deposited on the different ETMs are similar with small increase in intensity in the PL spectra of F8BT/POM interfaces. Figures 3b,c provide the exciton lifetimes of F8BT on the various electron transport layers determined by transient PL measurements at emission wavelengths 530 and 570 nm, respectively. Detecting at two emission wavelengths (530 and 570 nm) was applied to probe the dynamics of higher and lower energy excitons in order to determine the effect of the substrate on different transitions. Specifically, the 530 nm detection corresponds to the peak of the PL spectrum while 570 nm is located at the long wavelength tail, thus probing the dynamics of the relaxed excitons localized on low-energy species. The average exciton lifetime was obtained by fitting with a three-exponential decay function (Tables S1 and S2, Supporting Information) since the fitting of the PL decays with a single- or bi-exponential decay function gave unacceptable results. How good the fitting is can be determined through the χ^2 parameter which should be less than 1.1 for an acceptable fitting. Using the multiexponential

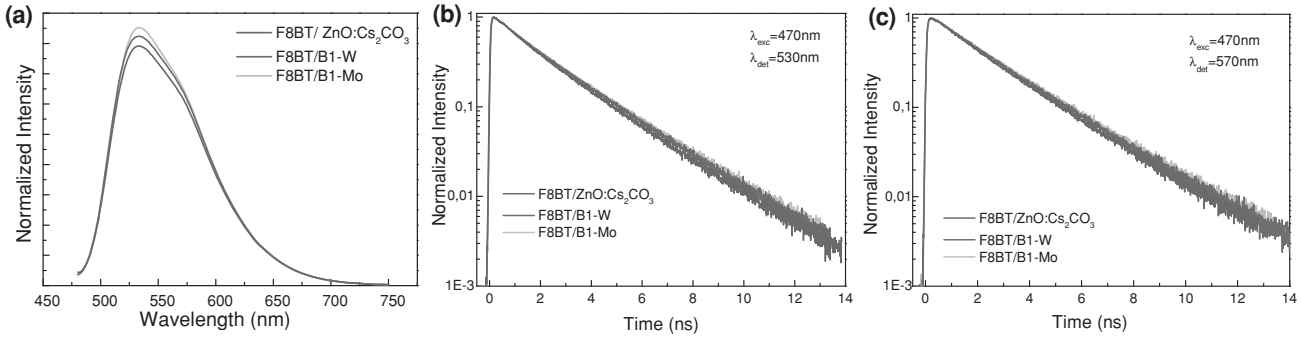

Figure 3. a) PL spectra of the F8BT on the three different ETMs, b,c) PL dynamics, detected at 530 and 570 nm, respectively, of F8BT on different substrates consisting of the electron transport materials studied here.

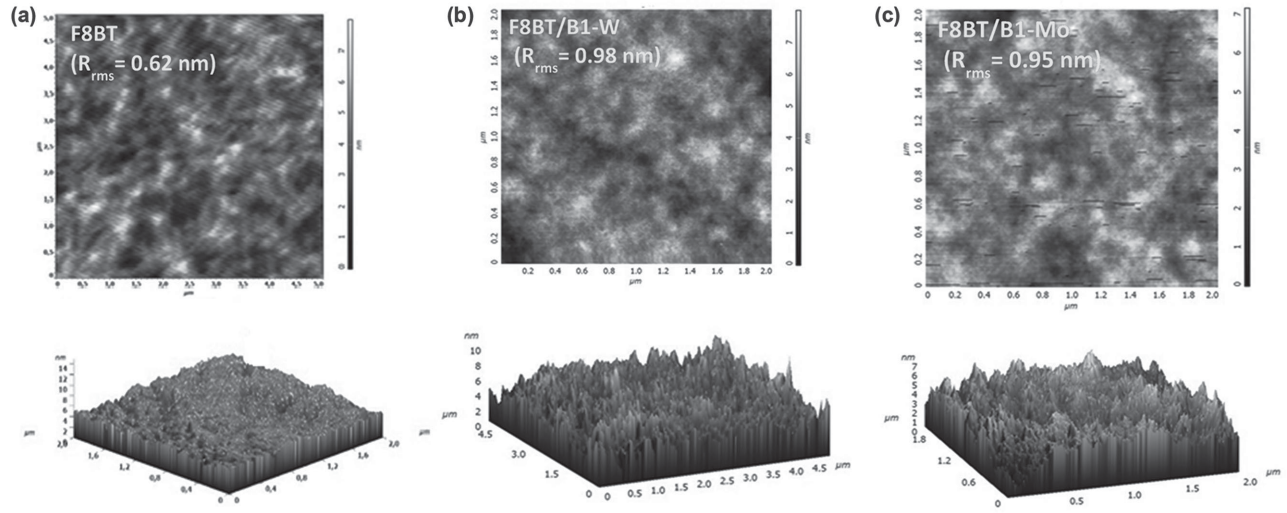

Figure 4. 2D AFM (2 × 2) topographies of F8BT films covered with the different POM materials with an approximate thickness of 20 nm.

function for fitting the decays means that there is a distribution of emitting states and decay mechanisms possibly due to different packing conformations of the emitting polymer and/or energy migration among adjacent chains with different conjugation lengths. The most efficient mechanism is found at 1.8–2.1 ns with amplitude ranging from 0.51 to 0.76, depending on sample and detection wavelength implying that this is the main decay mechanism of the polymer. However, in such systems, the different time constants used in the parallel decay model, by means of a multiexponential function, do not necessarily correspond to physical mechanisms and therefore it is more straightforward to discuss and compare the average decay times of the samples. These average exciton lifetimes of F8BT on B1-W, B1-Mo, and ZnO:Cs_2CO_3 were 1.90, 1.96, and 1.83 ns at 530 nm, and 2.11, 2.18, and 1.90 ns at 570 nm, respectively, whereas that of the pristine F8BT was 1.86 and 1.98 ns, respectively (Tables S1 and S2, Supporting Information). It is evident that in all cases the exciton lifetimes of F8BT on POMs are longer than those of the pristine F8BT (and even longer than those of F8BT on ZnO:Cs_2CO_3) which is a clear evidence of reduced exciton quenching and increased exciton lifetime at the F8BT/POM interfaces.[63,64] The above results indicate the confinement of excitons in the emissive layer which is an additional benefit of using POMs as the ETMs leading to an enhanced performance of the F8BT OLED devices.

We also used atomic force microscopy (AFM) to investigate the surface morphology of POMs on top of the F8BT layer to understand if their surface topography underlies the observed trends in electron transport and in efficiency of the F8BT based OLEDs. **Figure 4** shows the 2D and the corresponding 3D topographical surface topographies of pristine F8BT and the two 20-nm thick POM films deposited on top of an F8BT film. It is evident that all films have smooth surfaces with root-mean-square (RMS) values of surface roughness 0.62 nm (F8BT), 0.98 nm (B1-W on F8BT), and 0.95 nm (B1-Mo on F8BT). However, despite the small RMS values of POM films, we can clearly see from their 3D surface morphology shown in Figure 4 that they form vertically aligned nanopillars (nanoprotrusions) which suggest that the area of POM/Al cathode contact is maximized, thus facilitating electron injection. The observed nanopillar morphology of our POMs implies that maximum charge transport can be expected in the vertical direction, which is consistent with measured high electron currents in our devices (Figure S5, Supporting Information). This is because nanoscale protrusions at the electrode surfaces in organic optoelectronics have been shown to dramatically improve the efficiency of charge carrier transport from/to the external circuit and that the origin of this improvement is the local amplification of the electrostatic field in the vicinity of these protrusions.[65] However, AFM topographies with high RMS roughness are also obtained in ZnO:Cs_2CO_3/F8BT interfaces (not shown) suggesting that the enhancement in the efficiencies of the devices with POM ETMs in comparison with the reference one should be sought elsewhere.

We next fabricated all solution-processed PHOLEDs with polymer-based blue phosphorescent emissive layer (PVK:OXD-7:10% FIrpic) and water solution deposited POM as the ETM. A reference device with the TmPyPB:Cs_2CO_3 deposited from a formic acid:water (3:1) solution to serve as ETM, was also fabricated.[20] **Figure 5** shows the performances of PHOLEDs with the different ETMs which are summarized in **Table 2**. The reference device with TmPyPB:Cs_2CO_3, despite the fact that it is already performing quite well, shows, however, a higher turn-on voltage of 4.8 V and lower current density and luminance as compared with the device with the B1-W (V_{on} = 4.5 V) and especially with the B1-Mo (V_{on} = 4.2 V) as ETMs (Figure 5a). The higher current densities at low voltages of the devices with POMs imply that charge injection from cathode has been further improved. The devices with POMs also showed increased power efficiencies (12.0 and 12.5 lm W^{-1} for the devices with B1-W and B1-Mo, respectively, Figure 5b) and luminous efficiencies/external quantum efficiencies (28.8 cd A^{-1}/14.8% and 30.0 cd A^{-1}/15.4% for the devices with B1-W and B1-Mo, respectively, Figure 5c) when compared with the reference device (10.0 lm W^{-1} and 24.0 cd A^{-1}/12.3%, respectively). The blue PHOLED

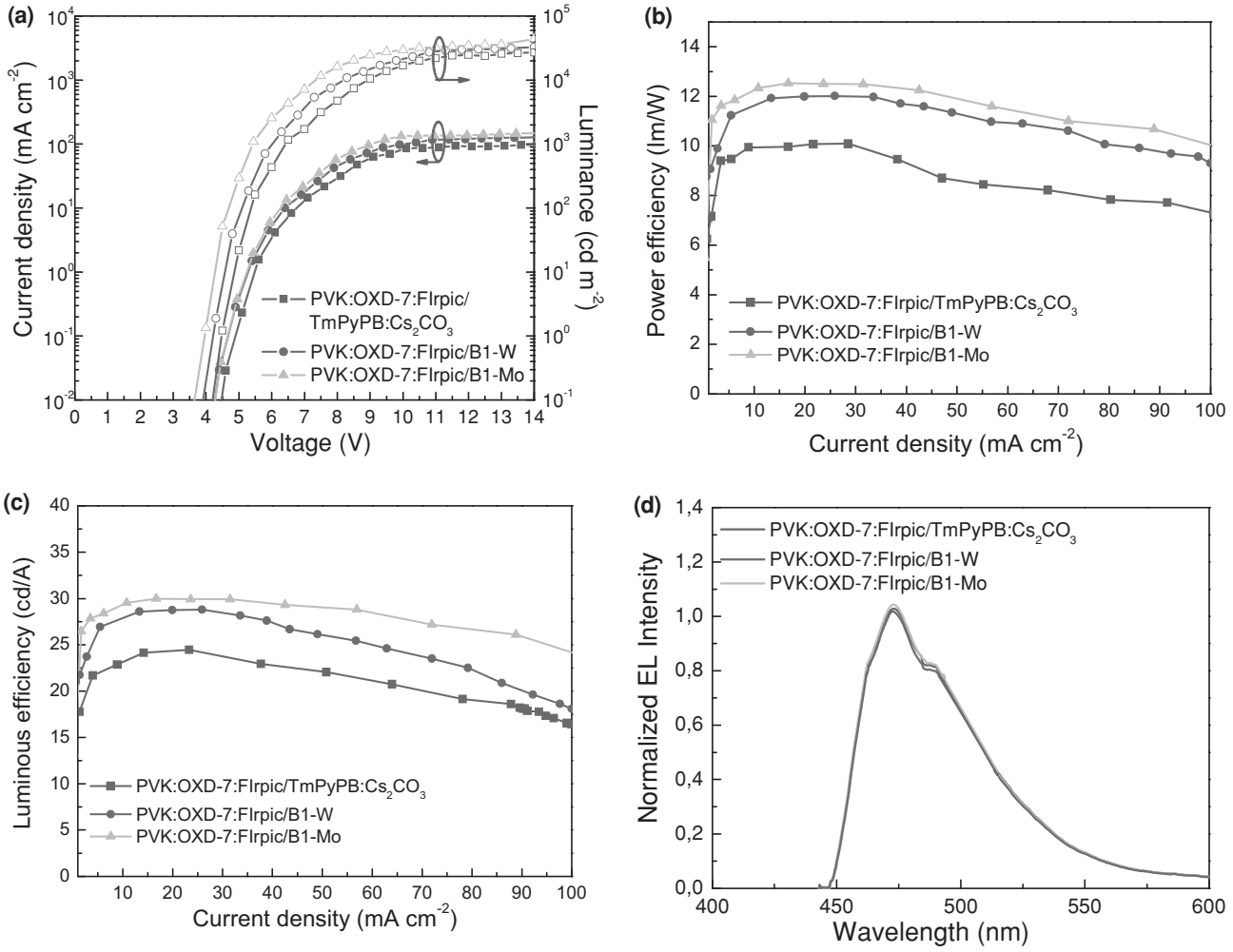

Figure 5. a) Current density and luminance versus voltage (*J–V–L*) characteristics, b) power efficiency, c) luminous efficiency versus current density, and d) EL spectra of blue PHOLEDs with different ETMs.

with B1-Mo showed the highest overall efficiency which is more than 25% better when compared with the reference device. The EL spectra of all the blue PHOLEDs are identical (Figure 5d) with a maximum peak at 472 nm which originates from FIrpic triplet emitter indicating effective confinement of carriers within the EML.[66] The Commission Internationale De L′ Eclairage coordinates of the devices were also identical (0.14, 0.28). Taking into account these results and also that our reference devices using Cs_2CO_3-doped TmPyPB to enhance electron injection/transport are already between the most efficient devices of their kind,[20] we support that water solution-processed lacunary POMs are excellent electron injection/transport layers for OLED devices with high efficiency and working stability.

As mentioned earlier, the turn-on—and also driving voltages—of the OLED devices with POMs are lower than those of the reference devices and much lower than those of previously reports FIrpic-based devices.[67] At first, we speculate that these decreased values can be attributed to a low electron injection barrier for ETMs of B1-W and B1-Mo. To let aside speculations and evaluate energy levels of POMs, their ultra-violet photoelectron (UPS) spectra when deposited on ITO substrates were measured and shown in **Figure 6**a,b for B1-W and B-Mo, respectively; on the left part and right part of each spectrum the

Table 2. Device characteristics of phosphorescent OLEDs having the structure ITO/MoO_x/PVK:OXD-7:FIrpic/POM or TmPyPB:Cs_2CO_3/Al.

ETM	$V_{turn\text{-}on}$ [*V*] [at 1 cd m^{-2}]	J_{max} [mA cm^{-2}]	L_{max} [cd m^{-2}]	LE_{max} [cd A^{-1}]	PE_{max} [lm W^{-1}]	EQE_{max} [%]
TmPyPB:Cs_2CO_3	4.8	100	24 000	24.0	10.0	12.3
B1-W	4.5	120	34 500	28.8	12.0	14.8
B1-Mo	4.2	140	42 000	30.0	12.5	15.4

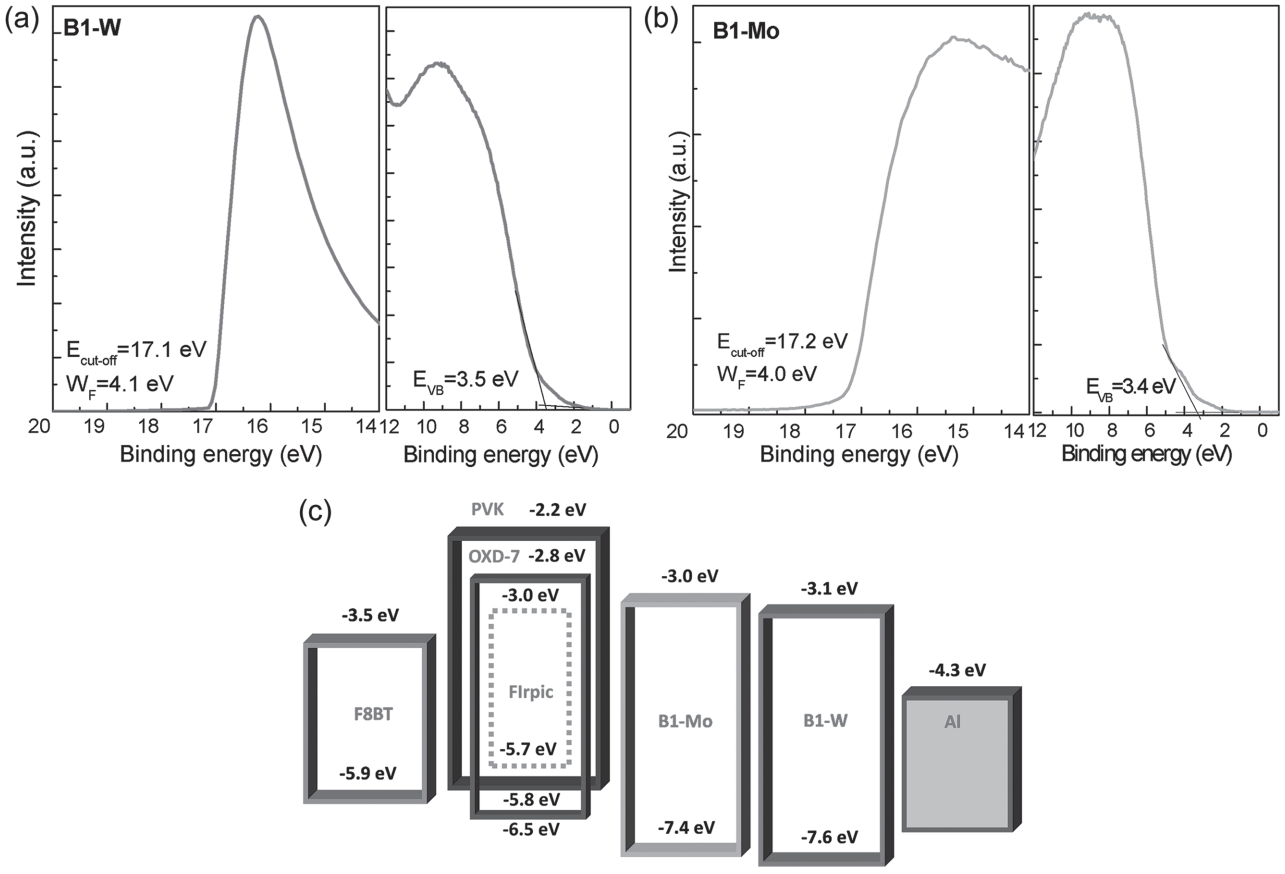

Figure 6. UPS spectra of a) B1-W and b) B1-Mo films with an approximate thickness of 20 nm deposited on ITO substrates. c) The energy level diagram of different materials used in the OLED devices.

secondary electron cut-off and an expanded view of the valence band region, respectively, are shown. The work function (W_F) of each sample surface can be directly obtained by measuring the secondary electron cut-off of the photoemission spectra which gives a W_F value of 4.1 and 4.0 eV for B1-W and B-Mo, respectively. These values are lower than the W_F of Al cathode which means that, unlike our previous studies,[56] these POMs could not be reduced by Al and therefore the mechanism(s) for enhanced electron injection and transport should be sought elsewhere. By adding the binding energy (BE) of the onset of the band of occupied orbitals (also called as the oxo band) the ionization energy (I_E) of each POM was estimated (having values 7.6 and 7.4 eV, respectively) which gives the position of the highest occupied molecular orbital (HOMO) with respect to the vacuum level. Based on these UPS results, a molecular orbitals scheme for the POMs studied here is presented in Figure 6c, where the position of the *oxo* band (HOMO) in each POM is associated with the ionization energy estimated from the UPS measurements. The position of the LUMO level is derived by taking into account the HOMO–LUMO energy differences (energy gap values) estimated by UV–vis absorption spectra analysis (Figure S7, Supporting Information). The energy levels of the materials used in EMLs were taken from the literature.[68,69] For simplicity reasons vacuum level alignment is considered.

It is concluded that in all cases the LUMO level of POM lies between the Fermi level of Al (which is equal to 4.3 eV) and the LUMO level of the emissive component, resulting therefore in decreased electron injection barrier. The slightly higher LUMO level of B1-Mo compared with that of B1-W may enable a lower electron injection barrier to the LUMO of the emissive component and better device performance. It is noteworthy that in the case of phosphorescent emissive layer, the LUMO level of B1-Mo is aligned with that of FIrpic emitter, which can explain the better performance of the blue PHOLED with the particular ETM. Furthermore, the deep HOMO level of POMs results in a large barrier for hole extraction at the cathode contact which makes POMs exceptional hole blocking layers for the both types of OLED devices. However, by taking into account the LUMO position of our POMs, a large electron injection barrier should be present at the POM/Al cathode contact interfaces. Such a large energy barrier should hamper electron injection from the cathode and deteriorate the performance of our devices which is not the case here. On the contrary, enhanced electron injection is supported by the *J–V* curves presented in Figure S5 (Supporting Information). We believe that these POMs act as "ionic electrets" (charged species) due to their macroscopic surface electrostatic charge resulting from their distorted (asymmetric) lacunary structure.[70] Consequently, a large permanent dipole within the POM layer may be formed resulting also in

the formation of a favorable interfacial dipole at the Al/POM interface (with its negative pole pointing toward Al) that could facilitate electron injection. This may be corroborated by the UPS results discussed above (Figure 6), according to which an effective reduction of the ITO workfunction of ≈0.4–0.5 eV is observed upon coating a charged POM overlayer. A similar dipole may be formed at the Al/POM interface and facilitate interfacial energy level alignment across this interface. The favorable energy level alignment at the POM/F8BT and POM/FIrpic interfaces should then allow electrons to efficiently inject from POM to the LUMO of the organics. Another plausible mechanism that could also play a role is hole accumulation at the organic/POM interface, due to the large interfacial barrier for hole transport, that could screen the electric field in the active organic layer and, thus, further facilitate electron injection at the organic/POM/Al interfaces.[71] Finally, the enhanced local electric field due to the formation of nanoprotrusions in POM films, as discussed above, may also contribute to the reduction of electron injection barrier at the Al/POM interface. Moreover, the more efficient operation of OLEDs with POMs may also be due to high electron mobilities of B1-W and B1-Mo.

Electron mobilities of these materials were initially measured by using conventional time-of-flight (TOF) technique using a nitrogen laser at a wavelength of 337 nm. **Figure 7**a shows the electron photocurrent transients for B1-W and B1-Mo (0.9 μm thick). Both plots exhibit a plateau with a defined shoulder which makes finding transit time easy. The transit time was estimated to be ≈0.59 μs for B1-W and 0.36 μs for B1-Mo at an external bias of 20 V. Next, according to the Poole–Frenkel law, by plotting mobility as a function of the square root of electrical field E, a linear relation can be found between them in a log-log scale. Indeed, as shown in Figure 7b, the electron mobility of B1-W lays in the range from 2.9×10^{-3} to 8.5×10^{-3} cm^2 V^{-1} s^{-1}, at electric field between 2.5×10^5 to 6.4×10^5 V cm^{-1}. B1-Mo shows a higher electron mobility which ranges from 3.8×10^{-3} to 1.0×10^{-2} cm^2 V^{-1} s^{-1}, at electric fields between 2.5×10^5 to 6.4×10^5 V cm^{-1}. Both are more than three orders of magnitude higher than those of other electron transport materials like the well-known Alq3.[72] To the best of our knowledge, the electron mobilities of POMs presented here are the highest ones for solution processed ETMs in amorphous film state ever reported. This may be attributed to the fact that these POMs were found to be reduced as revealed from their X-ray photoelectron (XPS) spectra presented in Figure S8 (Supporting Information). These spectra were measured on POM films deposited on ITO substrates. According to these spectra, B1-W seems to incorporate two additional electrons within its structure whereas B1-Mo is slightly more reduced (which can explain the higher mobility).[56] Such degree of reduction may render these POMs to semi-metallic materials which can explain the high mobility values measured in these films.

However, because the thickness of the POM layers used for the TOF measurements was much higher (of the order of microns) than the typical value used in the OLEDs structure, we also performed space-charge-limited-current (SCLC) measurements to evaluate carrier mobility under a steady current state in the POM layers.[73–75] Figure S9 (Supporting Information) shows the current density-voltage characteristics of Al/POM (120 nm)/Al devices while Figure 7c shows the logarithmic J/E^2 versus the square root of the mean electric field. From these data the zero-field mobility can be extracted by using Equation (1)

$$J = \frac{9}{8}\varepsilon\varepsilon_0 \frac{E^2}{L}\mu_0 \exp(0.89\beta\sqrt{\mathrm{E}}) \quad (1)$$

where J is the current density, ε is the relative permittivity, ε_0 is the permittivity of free space, μ_0 is the zero-field mobility, E is the applied electric field (that obtained by dividing the applied voltage V to the thickness L = 120 nm of the POM layer) and β is the field activation factor. The field activation exponential factor β, which governs the voltage variation of the mobility, was found equal to 1.7×10^{-4} and 1.8×10^{-4} cm$^{1/2}$ V$^{-1/2}$, respectively, for B1-W and B1-Mo, whereas the zero-field electron mobilities were found equal to 1.7×10^{-3} and 2.6×10^{-3} cm^2 V^{-1} s^{-1}, respectively. Figure 7d also shows the field dependence of electron mobilities of 120-nm thick POM films as derived from SCLC measurements. It is evident that under the same electric fields as in the case of TOF measurements, the estimated electron mobility of POMs lays within similar ranges as before. In particular, the electron mobility of B1-W varies from 2.6×10^{-3} to 8.3×10^{-3} cm^2 V^{-1} s^{-1}, whereas that of B1-Mo ranges from 3.0×10^{-3} to 1.0×10^{-2} cm^2 V^{-1} s^{-1}. These results indicate that irrespective of the technique used to measured electron mobilities of POM films and the thicknesses of these films, the extracted values are always quite similar and exceptionally high. These high values are consistent with efficient device operation in both fluorescent and phosphorescent OLEDs as verified from our data.

3. Conclusions

We have demonstrated that two water-soluble lacunary polyoxometalates derived from the Keggin structure, the B1-W and B1-Mo, exhibit the benefits of excellent electron mobility, low electron affinity, and high ionization energy for use as electron transport materials in OLED devices. Highly efficient green fluorescent and blue phosphorescent OLEDs are achieved by using these POMs as the electron transport materials attributed to high electron transport rates derived from their excellent mobilities, improved electron injection, efficient hole blocking, and effective confinement of carriers and excitons within the emissive layer. Our work indicates that replacing commonly used electron transport layers combined with hole blocking layers by a simple POM electron transport layer is possible. From their beneficial energy levels and exceptional electron mobilities, application of POMs in a diverse range of fluorescent and phosphorescent devices can be expected. These results suggest that designing of an electron transport material in order to combine several desirable properties is an effective way to further improve performance of next generation OLED devices.

4. Experimental Section

Synthesis of B1-W POM Material: To synthesize the B1-W in a solution of $Na_2WO_4{\cdot}2H_2O$ (181.5 g, 0.550 mol) in 300 mL water, 50 mL of

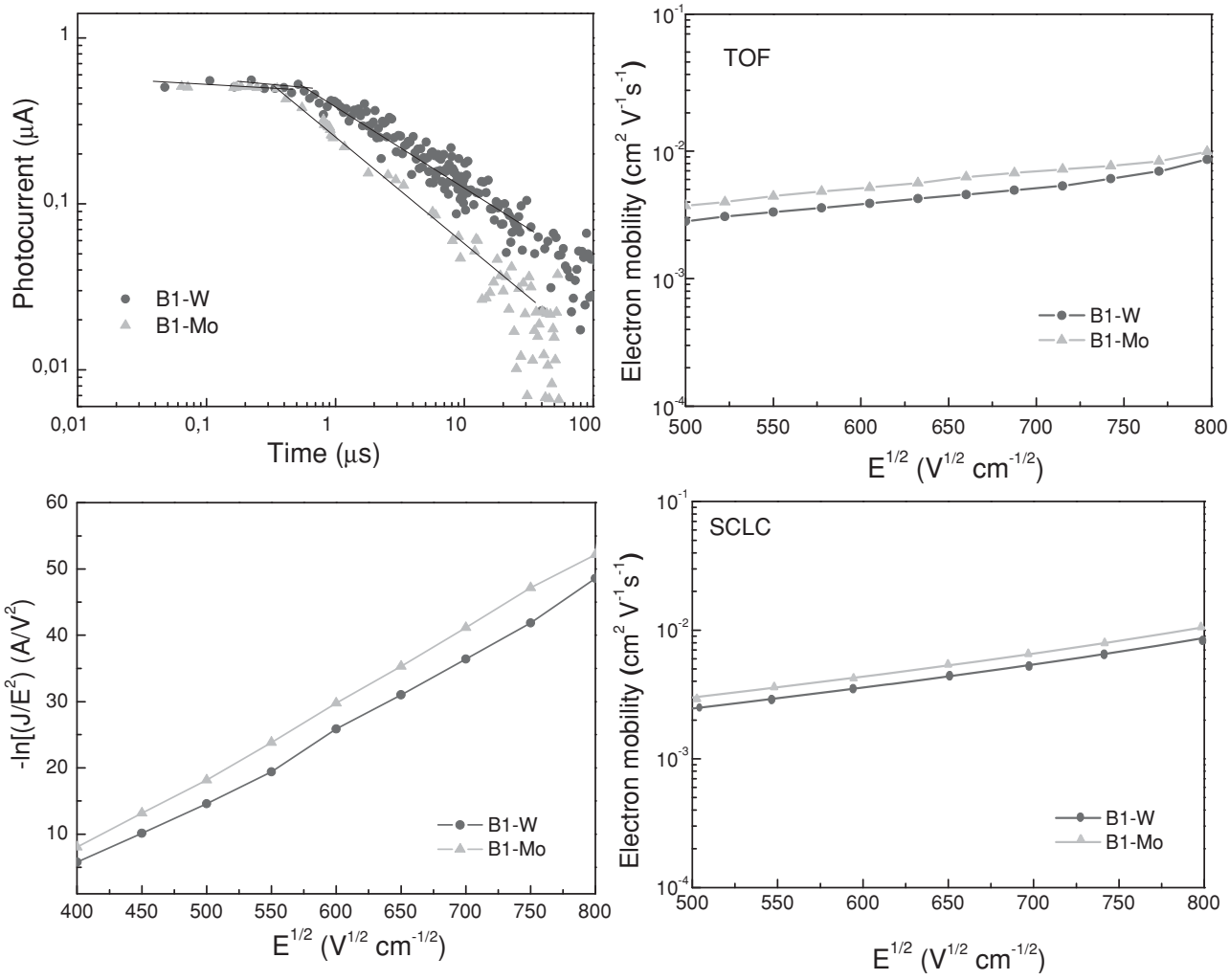

Figure 7. a) Time-of-flight (TOF) photocurrent transient for B1-W and B1-Mo shown in a log–log scale. b) Electron mobilities of B1-W and B1-Mo films plotted as a function of the square root of the electric field as derived from TOF measurements. c) Space-charge-limited-currents and d) electron mobilities versus the square root of the electric field as derived from the space-charge-limited-current measurements.

H_3PO_4 1 M, and 88 mL of glacial CH_3COOH were added. The solution was refluxed during 1 h, then KCl (60 g, 0.805 mol) was added; the white precipitate which appeared was filtered, washed with water, and dried in air to afford the B1-W.

Synthesis of B1-Mo POM Material: Similarly, in a solution of $Na_2MO_4{\cdot}2H_2O$ (133.04 g, 0.550 mol) in 220 mL water 36.6 mL of H_3PO_4 1 M, and 64.4 mL of glacial CH_3COOH were added. The solution was refluxed during 30 min, then KCl (43.8 g, 0.805 mol) was added; the white precipitate which appeared was filtered, washed with water, and dried in air to afford the B1-Mo.

Devices Preparation: OLEDs were fabricated on oxygen plasma-cleaned indium tin oxide (ITO) coated glass substrates. For the fluorescent devices, a solution processed molybdenum oxide (s-MoO_x) film was used as the HTL. Next, a ≈150-nm thick layer of the light-emitting green polyfluorene copolymer poly[(9,9-dioctylfluorenyl-2,7-diyl)-co-(1,4-benzo-{2,1′,3}-thiadiazole)] (obtained from American Dye Source Inc.) was spin-cast on s-MoO_x from a 15 mg mL^{-1} chloroform solution. Prior to spin coating, the polymer solution was filtered using a 0.20 μm PTFE filter. After spin coating, the emissive layer was annealed at 110 °C for 10 min in air. In order to enhance electron injection, a POM layer with a thickness of about 20 nm was deposited onto the polymer surface from a water solution via spin coating at 5000 rpm for 60 s without any post-annealing requirements. In addition, reference devices using a Cs_2CO_3-doped ZnO electron injection layers were fabricated. For the synthesis on ZnO nanoparticles, zinc acetate, water, and methanol were added to a flask and heated at 60 °C. Next, potassium hydroxide was dissolved into methanol and then added to the flask and the mixture was stirred for several hours. Then, a 10 mg mL^{-1} ZnO solution was prepared by dispersing the nanoparticles in 2-ethoxyethanol. The ZnO:Cs_2CO_3 solution was obtained by blending the ZnO solution with the Cs_2CO_3 solution (2 mg mL^{-1} in 2-ethoxy ethanol) in a 1:1 volume ratio. Then, the solution was spin coated at 4000 rpm to obtain a 10 nm ZnO:Cs_2CO_3 film. Finally, a 150-nm Al cathode was evaporated in a dedicated chamber.

In phosphorescent OLEDs, s-MoO_x was also used to make a 30-nm hole-injection layer onto a pre-cleaned ITO glass. The phosphorescent emissive layer consisted of a blend of poly(9-vinylcarbazole) (PVK) and 1,3-bis[2-(4-tert-butylphenyl)-1,3,4-oxadiazo-5-yl]benzene (OXD-7) (PVK:OXD-7 = 60:40, wt/wt) as a host and 10.0 wt% FIrpic as the blue dopant. The 70-nm polymer EML was obtained by spin coating of the PVK:OXD-7:FIrpic blend in chlorobenzene onto the s-MoO_x layer and vacuum dried at 100 °C. Then a 20-nm thick POM layer spun cast into the EML from a water solution, to enhance electron transport. For the fabrication of reference devices, the 1,3,5-tris(3-pyridyl-3-phenyl)benzene

(TmPyPB) materials was co-dissolved with Cs_2CO_3 in formic acid:water (3:1) solution and spun cast onto the EML at a spin speed of 7000 rpm followed by vacuum drying at 50 °C to form an ETL with a thickness of 20 nm. After drying, thermally evaporated Al cathode was deposited onto the ETL. All chemicals were purchased from Sigma-Aldrich and used without further purification.

Characterization Methods: Current density–voltage characteristics were measured with a Keithley 2400 source-measure unit. Luminance and EL spectra were recorded with an Ocean Optics USB 2000 fiber optic spectrophotometer, assuming a Lambertian emission profile (for luminance measurements). Surface morphology and structure of F8BT and F8BT/POM films were investigated with a Veeco AFM. All measurements were carried out in air at room temperature. The steady state PL spectra of F8BT on various ETLs were taken using a Fluoromax spectrometer (Horiba) upon excitation at 470 nm. The films were placed on a specific holder for solid samples and the spectra were corrected for the sensitivity of the detector. The PL dynamics were studied under magic angle conditions, by using a Time Correlated Single Photon Counting system (Fluotime, Picoquant) equipped with a Microchannel Plate photomultiplier. A pulsed diode laser at 470 nm was used for the excitation of the samples while the detection was at 530 (peak of the PL spectrum) and at 570 nm (low energy part of the PL spectrum). The Instrument's Response Function (IRF) was ≈80 ps. A three-exponential function convoluted with the IRF was used for fitting the dynamics. The time-of-flight measurements were made at room temperature and at electric fields ranging from 500 to 800 $(V\ cm^{-1})^{1/2}$. The current through the sample as a function of time was determined by using a storage oscilloscope to measure the voltage across a resistor placed in series with the sample. Five resistors varying in resistance from 50 Ω to 10 kΩ and several sweep speeds were used to cover several decades in time and current. All data for times shorter than ten RC time constants, where R is the series resistance and C is the sample capacitance, were discarded as invalid. The experimental results obtained for electrons in 900 nm thick POM layers with the illuminated electrode being negative corresponding to electron mobility measurement. Devices for SCLC measurements were fabricated with ITO/POM/Al structure. Current–voltage characteristics of SCLC devices were measured using the same semiconductor parameter analyzer as for OLED devices. The SCLC measurements were performed under dark and ambient conditions.The thicknesses of all films were measured with a J. A. Woollam spectroscopic ellipsometer in the following manner: the incident light wave from the ellipsometer strikes the surface of the film at an angle of θ_0, which will also be the angle of the reflected wave due to Snell's law. By using the appropriate model, the two ellipsometric parameters ψ and Δ, which are related to nine real parameters, are estimated. These parameters are the real and imaginary parts of the complex refractive indexes, $\tilde{n}_0$, $\tilde{n}_1$, $\tilde{n}_2$, the angle of incidence θ_0, the free-space wavelength of the incident light wave λ and the film thickness d. A set of ellipsometric parameters are measured at a given angle of incidence and a given wavelength and thus the thickness of the film is the only unknown, when the refractive indexes of the ambient, film, and substrate are known.

Supporting Information

Supporting Information is available from the Wiley Online Library or from the author.

Acknowledgments

This work was performed in the framework of "YDISE" project within GSRT's KRIPIS action, funded by Greece and the European Regional Development Fund of the European Union under NSRF 2007–2013 and the Regional Operational Program of Attica. The authors also thank Selcuk University Research Foundation (BAP PN: 14201047), TUBA, and DPT (PN: 2009K121080).

Received: November 11, 2015
Revised: January 8, 2016
Published online: February 25, 2016

[1] J. S C. W. Tang, S. A. Vanslyke, *Appl. Phys. Lett.* **1987**, *51*, 913.
[2] N. C. Greenham, S. C. Moratti, D. D. C. Bradley, R. H. Friend, A. B. Holmes, *Nature* **1993**, *365*, 628.
[3] J.-S. Kim, R. H. Friend, I. Grizzi, J. H. Burroughes, *Appl. Phys. Lett.* **2005**, *87*, 023506.
[4] F. So, J. Kido, P. Burrows, *MRS Bull.* **2008**, *33*, 663.
[5] S. Reineke, F. Lindner, G. Schwartz, N. Seidler, K. Walzer, B. Lussem, K. Leo, *Nature* **2009**, *459*, 234.
[6] Y. Kawamura, S. Yanagida, S. R. Forrest, *J. Appl. Phys.* **2002**, *92*, 87.
[7] C.-H. Yang, Y.-M. Cheng, Y. Chi, C.-J. Hsu, F.-C. Fang, K.-T. Wong, P.-T. Chou, C.-H. Chang, M.-H. Tsai, C.-C. Wu, *Angew. Chem. Int. Ed.* **2007**, *46*, 2418.
[8] T. Earmme, E. Ahmed, S. A. Jenekhe, *J. Phys. Chem. C* **2009**, *11*, 18448.
[9] E. Ahmed, T. Earmme, G. Ren, S. A. Jenekhe, *Chem. Mater.* **2010**, *22*, 5786.
[10] C. Adachi, *Appl. Phys. Lett.* **2011**, *98*, 083302.
[11] V. Coropceanu, J.-L. Brédas, B. Kippelen, S. Marder, *Chem. Mater.* **2011**, *23*, 4002.
[12] T.-W. Lee, T. Noh, H.-W. Shin, O. Kwon, J.-J. Park, B.-K. Choi, M.-S. Kim, D. W. Shin, Y.-R. Kim, *Adv. Funct. Mater.* **2009**, *19*, 1625.
[13] R. H. Friend, R. W. Gymer, A. B. Holmes, J. H. Burroughes, R. N. Marks, C. Taliani, D. D. C. Bradley, D. A. Dos Santos, J. L. Bredas, M. Logdlund, W. R. Salaneck, *Nature* **1999**, *397*, 121.
[14] L. Duan, L. Hou, T.-W. Lee, J. Qiao, D. Zhang, G. Dong, L. Wang, Y. Qiu, *J. Mater. Chem.* **2010**, *21*, 6392.
[15] B. Ma, B. J. Kim, D. A. Poulsen, S. J. Pastine, J. M. J. Fréchet, *Adv. Funct. Mater.* **2009**, *19*, 1024.
[16] S. C. Lo, R. N. Bera, R. E. Harding, P. L. Burn, I. D. W. Samuel, *Adv. Funct. Mater.* **2008**, *18*, 3080.
[17] J.-H. Jou, W.-B. Wang, S.-M. Shen, S. Kumar, I. M. Lai, J.-J. Shyue, S. Lengvinaite, R. Zostautiene, J. V. Grazulevicius, S. Grigalevicius, S.-Z. Chen, C.-C. Wu, *J. Mater. Chem.* **2011**, *21*, 9546.
[18] A. J. Clulow, C. Tao, K. H. Lee, M. Velusamy, J. A. McEwan, P. E. Shaw, N. L. Yamada, M. James, P. L. Burn, I. R. Gentle, P. Meredith, *Langmuir* **2014**, *30*, 11474.
[19] S. Ohisa, Y.-J. Pu, N. L. Yamada, G. Matsuba, J. Kido, *ACS Appl. Mater. Interfaces* **2015**, *7*, 20779.
[20] T. Earmme, S. A. Jenekhe, *Adv. Funct. Mater.* **2012**, *22*, 5126.
[21] T. Earmme, S. A. Jenekhe, *J. Mater. Chem.* **2012**, *22*, 4660.
[22] T. Earmme, S. A. Jenekhe, *Appl. Phys. Lett.* **2013**, *102*, 233305.
[23] G. Liu, A.-Y. Li, D. An, H.-B. Wu, X.-H. Zhu, Y. Li, X.-Y. Miao, W.-L. Deng, W. Yang, Y. Cao, J. Roncali, *Macromol. Rapid Commun.* **2009**, *30*, 1484.
[24] L. S. Hung, C. W. Tang, M. G. Mason, *Appl. Phys. Lett.* **1997**, *70*, 152.
[25] X. Gong, M. R. Robinson, J. C. Ostrowski, D. Moses, G. C. Bazan, A. J. Heeger, *Adv. Mater.* **2002**, *14*, 581.
[26] F. So, B. Krummacher, M. K. Mathai, D. Poplavskyy, S. A. Choulis, V. E. Choong, *J. Appl. Phys.* **2007**, *102*, 091101.
[27] X. H. Yang, F. Jaiser, S. Klinger, D. Neher, *Appl. Phys. Lett.* **2006**, *88*, 021107.
[28] Y. Li, D. Q. Zhang, L. Duan, R. Zhang, L. D. Wang, Y. Qiu, *Appl. Phys. Lett.* **2007**, *90*, 012119.
[29] A. Gassmann, C. Melzer, E. Mankel, W. Jaegermann, H. Seggern, *J. Appl. Phys.* **2009**, *105*, 124517.

[30] H. J. Bolink, E. Coronado, J. Orozco, M. Sessolo, *Adv. Mater.* **2009**, *21*, 79.
[31] S. A. Haque, S. Koops, N. Tokmoldin, J. R. Durrant, J. S. Huang, D. D. C. Brandley, E. Palomares, *Adv. Mater.* **2007**, *19*, 683.
[32] N. Tokmoldin, N. Griffiths, D. D. C. Bradley, S. A. Haque, *Adv. Mater.* **2009**, *21*, 3475.
[33] H. J. Bolink, E. Coronado, D. Repetto, M. Sessolo, E. M. Barea, J. Bisquert, G. Garcia-Belmonte, J. Prochazka, L. Kavan, *Adv. Funct. Mater.* **2008**, *18*, 145.
[34] Y. Kawamura, S. Yanagida, S. R. Forrest, *J. Appl. Phys.* **2002**, *92*, 87.
[35] S. Reineke, K. Walzer, K. Leo, *Phys. Rev. B* **2007**, *75*, 125328.
[36] B. Walker, A. Tamayo, J. Yang, J. Z. Brzezinski, T.-Q. Nguyen, *Appl. Phys. Lett.* **2008**, *93*, 063302.
[37] S. O. Jeon, S. E. Jang, H. S. Son, J. Y. Lee, *Adv. Mater.* **2011**, *23*, 1436.
[38] C. Adachi, *Appl. Phys. Lett.* **2011**, *98*, 08330.
[39] V. Coropceanu, J.-L. Brédas, B. Kippelen, S. Marder, *Chem. Mater.* **2011**, *23*, 4002.
[40] M. Vasilopoulou, A. M. Douvas, D. G. Georgiadou, V. Constantoudis, D. Davazoglou, S. Kennou, L. C. Palilis, D. Daphnomili, A. G. Coutsolelos, P. Argitis, *Nanoresearch* **2014**, *7*, 679.
[41] S. M. Yoon, S. J. Lou, S. Loser, J. Smith, L. X. Chen, A. Facchetti, T. Marks, *Nano Lett.* **2012**, *12*, 6315.
[42] S.-J. Su, T. Chiba, T. Takeda, J. Kido, *Adv. Mater.* **2008**, *20*, 2125.
[43] T. Ye, S. Shao, J. Chen, L. Wang, D. Ma, *ACS Appl. Mater. Interfaces* **2011**, *3*, 410.
[44] T. Earmme, E. Ahmed, S. A. Jenekhe, *Adv. Mater.* **2010**, *22*, 4744.
[45] T.-W. Lee, T. Noh, H.-W. Shin, O. Kwon, J.-J. Park, B.-K. Choi, M.-S. Kim, D. W. Shin, Y.-R. Kim, *Adv. Funct. Mater.* **2009**, *19*, 1625.
[46] M. T. Pope, A. Müller, *Angew. Chem. Int. Ed. Engl.* **1991**, *30*, 34.
[47] M. T. Pope, *Heteropoly and Isopoly Oxometalates*, Springer-Verlag, Berlin, Germany **1983**.
[48] A. Hiskia, A. Mylonas, E. Papaconstantinou, *Chem. Soc. Rev.* **2001**, *30*, 62.
[49] J. Lehmann, A. Gaita-Arino, E. Coronado, D. Loss, *Nat. Nanotechnol.* **2007**, *2*, 312.
[50] A. Dolbecq, E. Dumas, C. R. Mayer, P. Mialane, *Chem. Rev.* **2010**, *110*, 6009.
[51] J. M. Clemente-Juan, E. Coronado*Coord. Chem. Rev.* **1999**, *193–195*, 361.
[52] T. He, J. Yao, *Prog. Mater. Sci.* **2006**, *51*, 810.
[53] A. M. Douvas, E. Makarona, N. Glezos, P. Argitis, J. A. Mielczarski, E. Mielczarski, *ACS Nano* **2008**, *2*, 733.
[54] P. Kogerler, B. Tsukerblat, A. Müller, *Dalton Trans.* **2010**, *39*, 21.
[55] L. C. Palilis, M. Vasilopoulou, D. G. Georgiadou, P. Argitis, *Org. Electron.* **2010**, *11*, 887.
[56] M. Vasilopoulou, A. M. Douvas, L. Palilis, S. Kennou, P. Argitis, *J. Am. Chem. Soc.* **2015**, *137*, 6844.
[57] A. Soultati, A. M. Douvas, D. G. Georgiadou, L. C. Palilis, T. Bein, J. M. Feckl, S. Gardelis, M. Fakis, S. Kennou, P. Falaras, T. Stergiopoulos, N. A. Stathopoulos, D. Davazoglou, P. Argitis, M. Vasilopoulou, *Adv. Energy Mater.* **2014**, *4*, 1300896.
[58] R. Contant, *Can. J. Chem.* **1987**, *65*, 568.
[59] T. Chiba, Y.-J. Pu, H. Sasabe, J. Kido, Y. Yang, *J. Mater. Chem.* **2012**, *22*, 22769.
[60] T. Chiba, Y.-J. Pu, J. Kido, *J. Mater. Chem. C* **2015**, *3*, 11567.
[61] J. Meyer, S. Hamwi, M. Kröger, W. Kowalsky, T. Riedl, A. Kahn, *Adv. Mater.* **2012**, *24*, 5408.
[62] M. Sessolo, H. J. Bolink, *Adv. Mater.* **2011**, *23*, 1829.
[63] B. R. Lee, E. D. Jung, J. S. Park, Y. S. Nam, S. H. Min, B.-S. Kim, K.-M. Lee, J.-R. Jeong, R. H. Friend, J.-S. Kim, S. O. Kim, M. H. Song, *Nat. Commun.* **2014**, *5*, 4840.
[64] L. P. Lu, D. Kabra, R. H. Friend, *Adv. Funct. Mater.* **2012**, *22*, 4165.
[65] L.-J. Pegg, R. A. Hatton, *ACS Nano* **2012**, *6*, 4722.
[66] T. W. Kwon, M. M. Alam, S. A. Jenekhe, *Chem. Mater.* **2004**, *16*, 4657.
[67] M.-H. Tsai, H.-W. Lin, H.-C. Su, T. H. Ke, C.-C. Wu, F.-C. Fang, Y.-L. Liao, K.-T. Wong, C.-I. Wu, *Adv. Mater.* **2006**, *18*, 1216.
[68] X. F. Ren, J. Li, R. J. Holmes, P. I. Djurovich, S. R. Forrest, M. E. Thompson, *Chem. Mater.* **2004**, *16*, 4743.
[69] D. Kolosov, V. Adamovich, P. Djurovich, M. E. Thompson, C. Adachi, *J. Am. Chem. Soc.* **2002**, *124*, 9945.
[70] L. S. McCarty, G. M. Whitesides, *Angew. Chem. Int. Ed.* **2008**, *47*, 2188.
[71] M. Lu, P. de Bruyn, H. T. Nicolai, G.-J. A. H. Wetzelaer, P. W. M. Blom, *Org. Electron.* **2012**, *13*, 1693.
[72] H. Park, D.-S. Shin, H.-S. Yu, H.-B. Chae, *Appl. Phys. Lett.* **2007**, *90*, 203102.
[73] P. W. M. Blom, M. M. J. de Jong, J. J. M. Vleggaar, *Appl. Phys. Lett.* **1996**, *68*, 3308.
[74] W. Brutting, S. Berleb, A. G. Muckl, *Org. Electron.* **2001**, *2*, 1.
[75] G. G. Malliaras, J. R. Salem, P. J. Brock, C. Scott, *Phys. Rev. B* **1998**, *58*, R13411.